CHAPTER 3

MATERIALS AND METHODS

3.1 General

This chapter describes a brief overview of the materials, planning, instrumentation, experimental procedures and methodologies. The type of materials and their basis for selection have been discussed. Several geotechnical properties of the test material were investigated along with the impact of hydrocarbon contamination on those properties. Some physical properties of the crude oil used as the contaminant were also evaluated. At last, various methods for liquefaction assessment have been summarized and the methodology adopted for this research has been discussed.

3.2 Soil Sampling

Soil sampling was done from three different locations of Assam, India. The state Assam consists of the major oil fields of India as such a vast land area there can be subjected to contamination problems. The sampling locations have been shown on the seismic hazard map on Assam in Fig. 3.1. The first sample (sample A) was collected from the nearby locations of Dibrugarh oilfield. Sample B was collected from the vicinity of Guwahati refinery and sample C was collected from the vicinity of Jorhat oil fields.

All the three samples were initially investigated for their relative susceptibility towards liquefaction as per the popularly used Chinese criterion presented in Table 3.1. Preliminary tests were done on all the three samples. Their respected gradation characteristics and liquid limit values have been tabulated and presented in Fig. 3.2. Based on the proposed criterion

and obtained results, sample B was identified to be the most liquefiable among the three while the sample C required further investigation. Therefore, sample B i.e. Guwahati sand was selected as the host sand for further investigation.

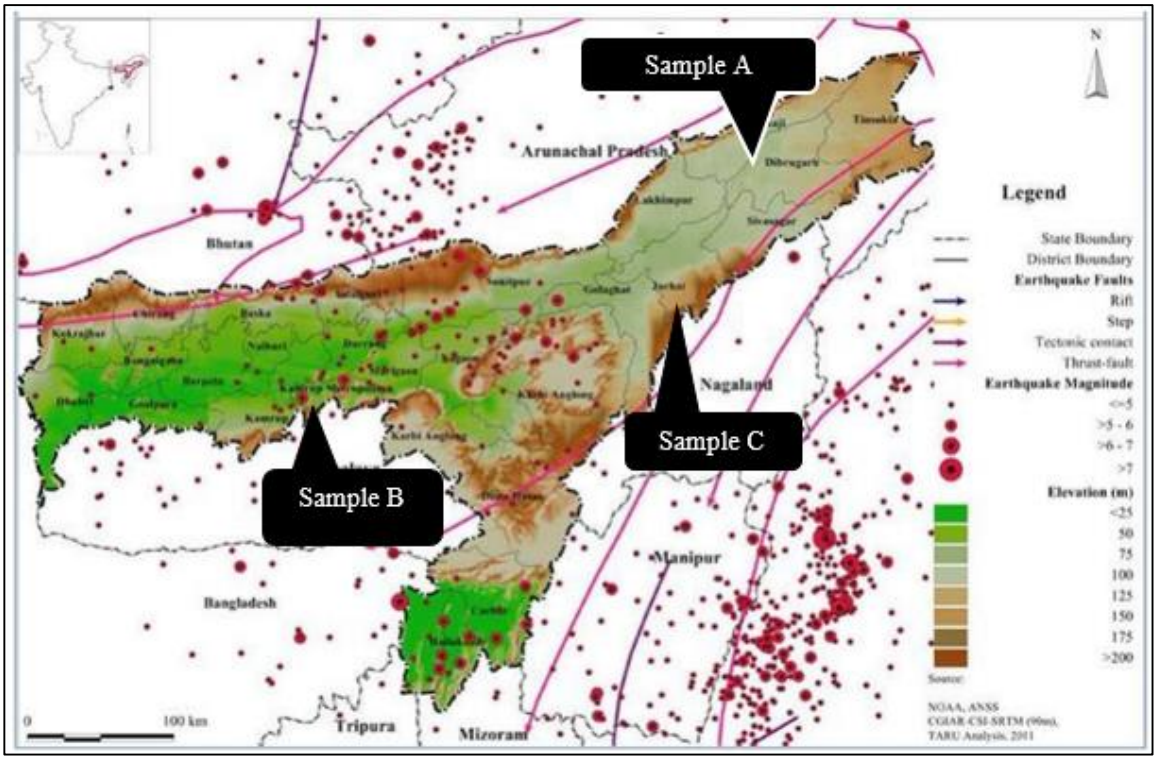

Fig. 3.1 Soil sampling locations in Assam, India (Source: National Disaster Risk Reduction Portal)

Table. 3.1 Chinese criterion for soil liquefaction

Clay Content	Liquid Limit < 32%	Liquid Limit ≥ 32%
< 10%	Susceptible	Further studies required For plastic, non-clay sized grain
≥10%	Further studies required for non-plastic clay sized grain	Not susceptible

Parameters	Sample A	Sample B	Sample C
Sand	39.24%	77%	42.65%
Silt	39.96%	22%	45.77%
Clay	20.8%	1%	11.58%
Liquid Limit	32.13%	0%	30.35%
Plastic Limit	23.24%	NON-PLASTIC	
Plasticity Index	8.89%		
Liquefaction Susceptibility	NOT SUSCEPTIBLE	SUSCEPTIBLE	UNCERTAIN

Fig. 3.2 Chart indicating initial assessment of relative liquefaction susceptibility of three samples based on Chinese criterion

3.3 Crude Oil

Contamination of ground with light crude oil is believed to have more adverse impacts as light crude oil being less viscous can penetrate to a much greater extent. The petroleum hydrocarbon used in the study investigation was light crude oil supplied by Indian Oil Corporation Limited (IOCL), Barauni, India. Table 3.2 is a summary of the basic oil properties. The viscosity of the oil was determined using Brookfield viscometer in accordance with the standard test method in ASTM D2983-09 while for determining the specific gravity and API gravity hydrometer method in ASTM D1298-12(b) was followed.

Table 3.2 Properties of light crude oil

Properties	Viscosity (cp)	Specific Gravity	API gravity at 20°C	Salt content (g/m^3)
Value	19.52	0.865	25.26	30

3.4 Artificial Contamination of Sand

For preparing clean and contaminated sand samples, the sand specimens were firstly oven-dried so as to completely remove any existing amount of moisture in the sand. The sand was then uniformly mixed with crude oil at varying oil dosages of 2, 4, 6, 8, 10 and 12% (volume

by weight) and kept in sealed bags for one week to allow proper interaction of oil and soil. The above mentioned range of crude oil dosage was selected as per the basis of previous literature (Al-Sanad et al. 1995; Khamehchiyan 2007; Taqieddin 2017).

3.5 Geotechnical properties of Guwahati Sand

3.5.1 Particle Size Distribution

The sand appeared to be greyish in color with mostly sand particles on visual examination. Wet sieving was performed in which the sand was first washed through 75 μm sieve and the fraction coarser and finer than 75μm were collected and oven dried separately. Following it, mechanical sieving and hydrometer methods were used as per ASTMD6913 and ASTMD7928 to analyze coarser fractions and finer fractions respectively. A semi log curve was plotted between percentage finer and diameter of particle in mm as shown in Fig. 3.3. The sand has been classified as silty sand (SM) as per Unified Soil Classification System (USCS). Grain size distribution curve of Guwahati sand lies well within the boundaries of potentially liquefiable soil proposed by Tuschida (1970). The physical and geotechnical properties of Guwahati sand have been summarized in Table 3.3.

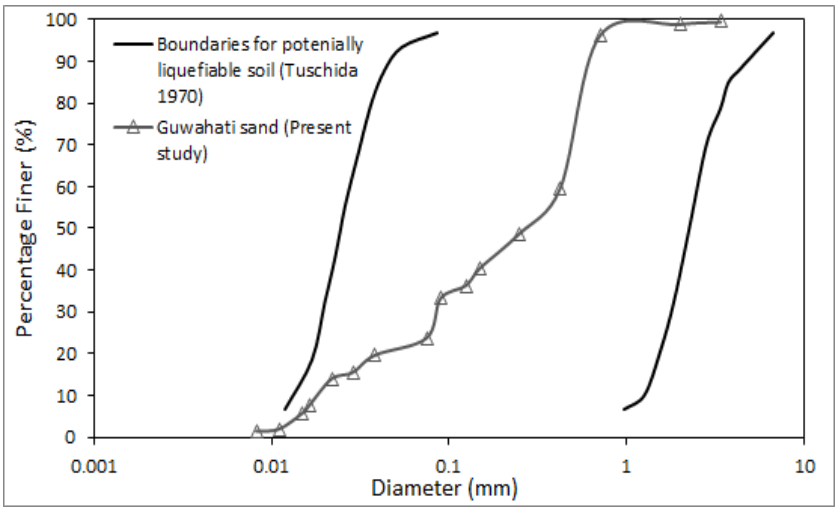

Fig. 3.3 Particle size distribution curve of Guwahati sand

Table 3.3. Basic geotechnical properties of Guwahati sand

Property	Value
Sand (%)	77.0
Silt (%)	22.0
Clay (%)	1.0
Angle of internal friction, ϕ	36^o
Cohesion (kPa)	2.8
Coefficient of uniformity, C_u	26.56
Coefficient of curvature, C_c	1.19
Maximum void ratio, e_{min}	0.439
Minimum void ratio, e_{max}	1.06
Soil Classification (USCS)	SM

3.5.2 Specific Gravity

The specific gravity of the clean and contaminated sands was measured using pycnometer in accordance with ASTM D854-14. For this, an empty pycnometer was cleaned and dried and its empty mass was taken (M_1) with its cap screwed tightly. The cap and pycnometer was marked with a vertical line parallel to the axis of the pycnometer to ensure that the cap is screwed to the same mark each time. Exactly 200gm of Guwahati sand was placed in the pycnometer and the cap was screwed to the mark. The mas of the pycnometer with sand was recorded (M_2). Again the cap was opened and sufficient amount of de-aired water was added so as to completely cover the sand. The cap was screed and the contents were shaken well. A vacuum pump was connected for 10-15 minutes to remove the entrapped air after which the pycnometer was filled completely with water up to the mark and its weight was recorded (M_3). Next, the pycnometer was completely filled with water only and its weight was again recorded (M_4). The specific gravity of soil was determined using the relation expressed in eq. (3.1)

$$G = \frac{M_2 - M_1}{(M_2 - M_1) - (M_3 - M_4)} \quad (3.1)$$

where M_1 = mass of empty Pycnometer, M_2 = mass of the Pycnometer with dry sand M_3 = mass of the Pycnometer and soil and water, M_4 = mass of Pycnometer filled with water only. G= Specific gravity of sand.

In case of hydrocarbon contaminated sands, the sand grains get coated with a layer of hydrocarbon which may not give the true specific gravity of the grains. Hence, apparent specific gravity was determined for contaminated sands while for uncontaminated sand, true specific gravity and apparent specific gravity would be same. Fig. 3.4 shows the variation of apparent specific gravity with the varying oil dosages and it is evident from the figure that there is a continuous dip in the apparent specific gravity with increasing oil content. The specific gravity of clean virgin sand was 2.67 while the same for ω= 8% was 2.36. Beyond ω =8% the dip was not significant.

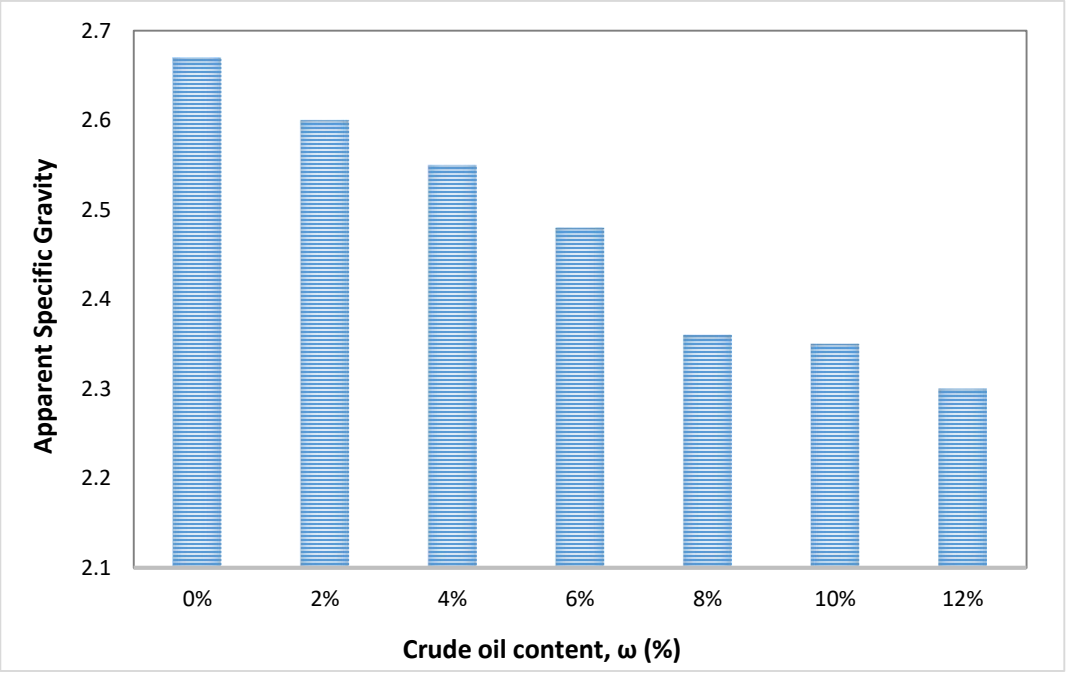

Fig. 3.4 Variation of apparent specific gravity with crude oil content

3.5.3 Compaction Characteristics

Modified compaction tests were carried out (ASTM D698) on clean Guwahati sand as well as on sand mixed with 2, 4, 6, 8, 10 and 12% (volume by weight) crude oil. A cylindrical metal mould with an inner diameter of 101.6 mm detachable collars and base plate was used for standard proctor test. For each compaction test, approximately 2.5 kg of sand was used. At first, the mould was cleaned, dried and greased to reduce friction on the sidewalls and its weight was recorded. It was then fixed to the base plate along with the collars. Required amount of water was then added into the sand (starting with 2% and then increasing with a step of 2%) and mixed thoroughly to balance the humidity. The sand was then compacted in three layers by applying 25 blows to each layer with a rammer of 2.5 kg in weight falling freely through a height of 305 mm. The surface of each layer was scarified before putting the next layer to facilitate proper interlocking of the layers. After compaction, the collar was removed and the excess soil was cut off to form a level surface. The weight of the compacted sand and mould was recorded. A small amount of sand specimen from top and bottom of the mould was taken out to determine its moisture content. The results were plotted in terms of maximum dry density and moisture content. The whole procedure was repeated for all oil contents and the effect of crude oil content on the compaction characteristics was evaluated. The compaction curves obtained for specimens corresponding to each oil content have been presented in Fig. 3.5. The curve shows a down and leftward shift with increasing oil contents. Fig.3.6 shows the variation of maximum dry density and optimum moisture content with crude oil content. It was observed from the figure that the OMC showed a continuous decrease with increasing oil content. The possible reason behind this decrease in OMC can be the oil which occupies the voids and reduces the water demand to reach the maximum dry

density. There was no considerable change in the maximum dry density up to 2% oil content. However, beyond 2% oil content, the maximum dry density reduces sharply with increasing oil content. This may be attributed to the capillary tension effect which is dominant at lower oil contents. Nevertheless, as oil content increases, capillary tension effect weakens and presence of excess oil in the voids restricts the sand particles to move around and get densely compacted.

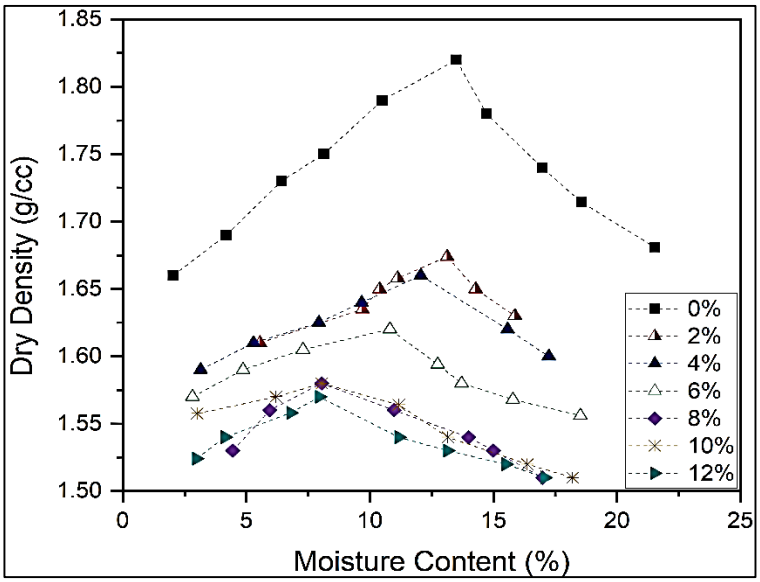

Fig. 3.5 Compaction curves for contaminated and uncontaminated sand

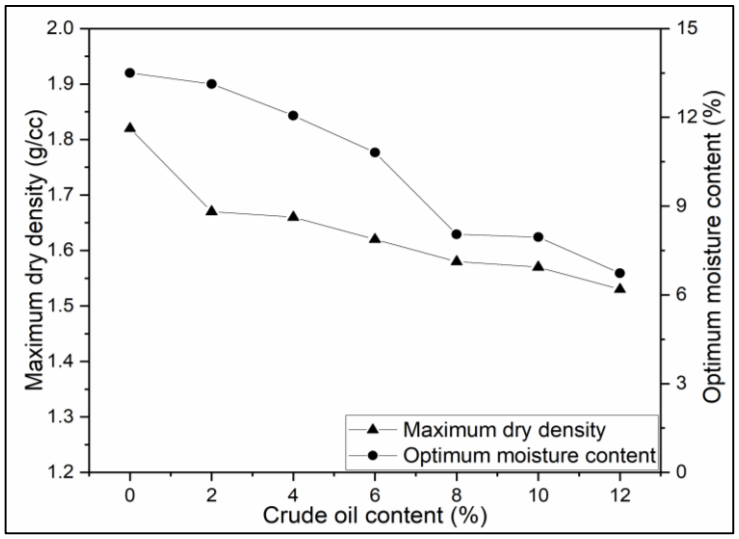

Fig. 3.6 Variation of OMC and MDD with crude oil content

One important point which can be debatable here is whether the OMC reported above corresponds to the moisture content or the fluid content as the soil matrix in such a case would consist of both oil and water. To address this, a separate oil evaporation study was conducted in which five different soil specimens were investigated under two different drying conditions for 21 days as shown in Fig. 3.7. For sample containing Sand+Oil+Water, a known amount of water (18% V/W) and oil (6% V/W) was mixed with sand. Similarly, for sample containing only Sand+Oil contains a known amount of oil (6% V/W). Both the samples were kept for oven drying. After 24 hours, the percentage loss in weight of sample containing Sand+Oil+Water was 18.95% while for the sample containing Sand + Oil was 0.9%. The results indicate that loss in weight of the specimen after oven drying was mainly due to loss of moisture and hence the term optimum moisture content can be interchangeably used for optimum fluid content.

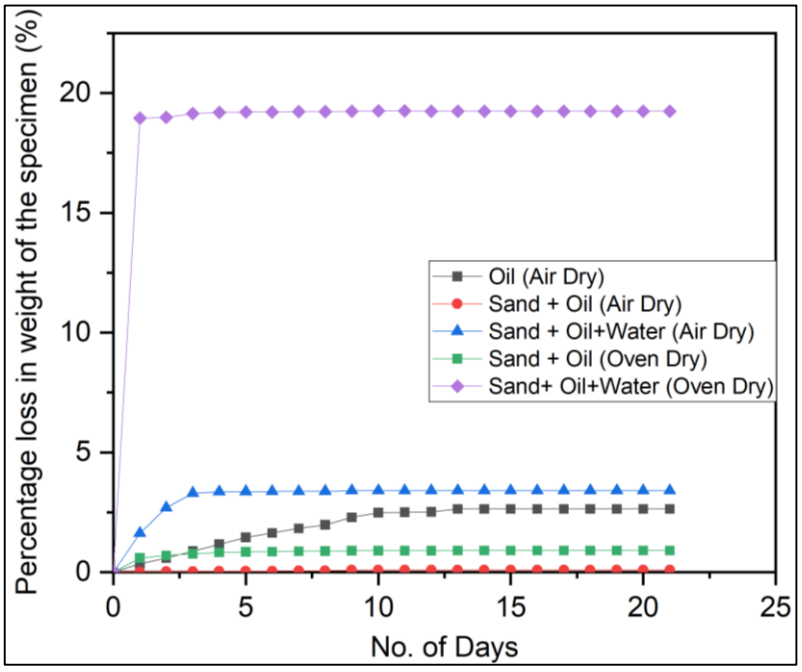

Fig. 3.7 Oil evaporation study of contaminated sand

3.5.4 Hydraulic Conductivity

Hydraulic Conductivity of the Guwahati sand was determined through conducting constant head permeameter in accordance with ASTM D2434 - 19. The sand was compacted in the permeability mould at OMC in 3 layers giving 25 blows for each layer with a 2.5 kg hammer. The mould with specimen inside shall be assembled to the drainage base and cap having porous discs. The porous discs were saturated prior assembling the mould. The assembly was then saturated with de-aired water from the bottom upwards under vacuum. After saturation, the specimen was connected through the top inlet to the constant head water reservoir. The bottom outlet was opened and when the steady state of flow was established, the quantity of flow for a convenient time interval was collected and measured. The collection of the quantity of flow for the same time interval was repeated thrice. The variation of hydraulic conductivity with crude oil content has been depicted in Fig. 3.8. The hydraulic conductivity of hydrocarbon contaminated sand gets reduced with increasing contamination. The reason can be attributed to the deposition of hydrocarbon into the soil pores which is a vital factor governing the soil permeability. It can also be further observed that increasing the amount of hydrocarbons effectively intensifies the degree of changes in permeability.

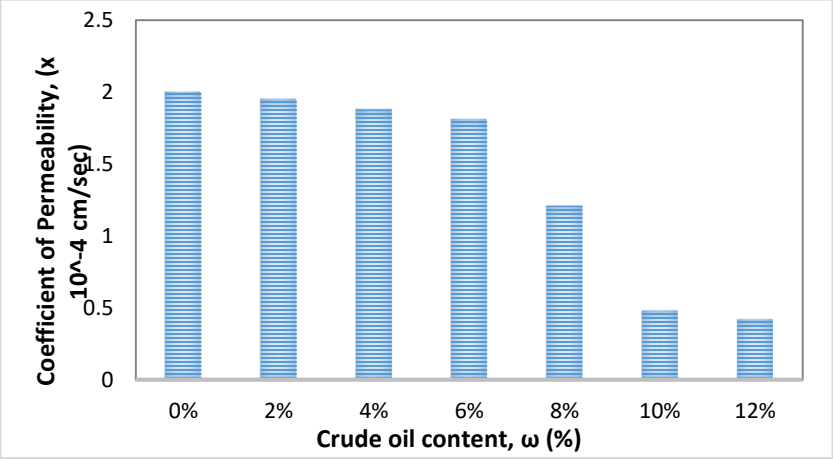

Fig. 3.8 Variation of coefficient of permeability with crude oil content

The change in coefficient of permeability when ω changed from 0% to 6 % was just 9.5%. On the other hand, when ω changed from 6% to 12%, the drop in the coefficient of permeability was 76.8%. The observed trend is in good agreement with the several past reported results (Akinwumi et al. 2014a; Akinwumi et al. 2014b; Al-Sanad et al. 1995; Budhu et al. 1991; Cook et al. 1992; Foreman and Daniel 1986; Khamehchiyan et al. 2007; Meegoda and Rajapakse 1993; Puri 2000; Puri et al. 1994; Rahman et al. 2010; Shin and Das 2000; Siang et al. 2014).

3.5.5 Triaxial Tests

Internal friction angle and cohesion resulting from inter-particle interactions are crucial factors that influence engineering behavior of soils. Therefore, identifying the impact of hydrocarbons on these parameters is an important aspect in learning more about their behavior. Consolidated drained triaxial tests were carried out (ASTMD7181-11) to compare the strength parameters of clean and contaminated sands at varying oil contents. Reconstituted cylindrical samples of diameter 36mm and length 72mm were prepared for clean and contaminated sand using split spoon sampler. The samples were prepared at their respective optimum moisture content.

The variation of peak friction angle and apparent cohesion with oil content have been plotted in Fig. 3.9. A careful observation of the figure indicates that there is a trivial decrease in peak friction angle up to 4% after which the dip was considerable. On the other hand, significant amount of cohesion seems to get developed due to the viscous effect of oil. This oil-induced cohesion was maximum at 6% after which it reduced sharply as the inter-granular spaces were excessively occupied with oil resulting into loss of grain to grain contact and breakdown of oil-induced tension forces.

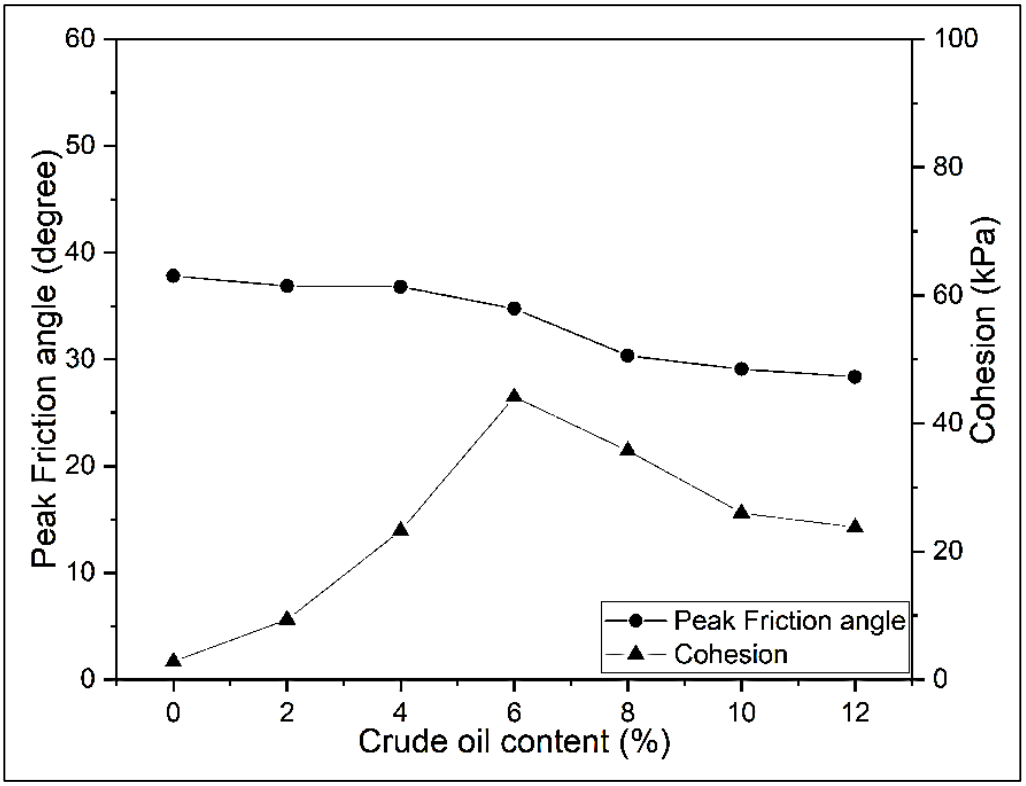

Fig. 3.9 Shear strength characteristics of uncontaminated and contaminated Guwahati sand

The stress- strain curves obtained for specimens at different oil contents have been shown in Fig. 3.10. The shown curves are evident of strain-softening behavior at initial oil dosages with a well-defined peak. Nevertheless, the intensity of these peaks gets suppressed with increasing oil contents exhibiting strain hardening effects. Moreover, the deviatoric stress gets reduced significantly with increasing oil content which justifies the decline in the peak friction angle.

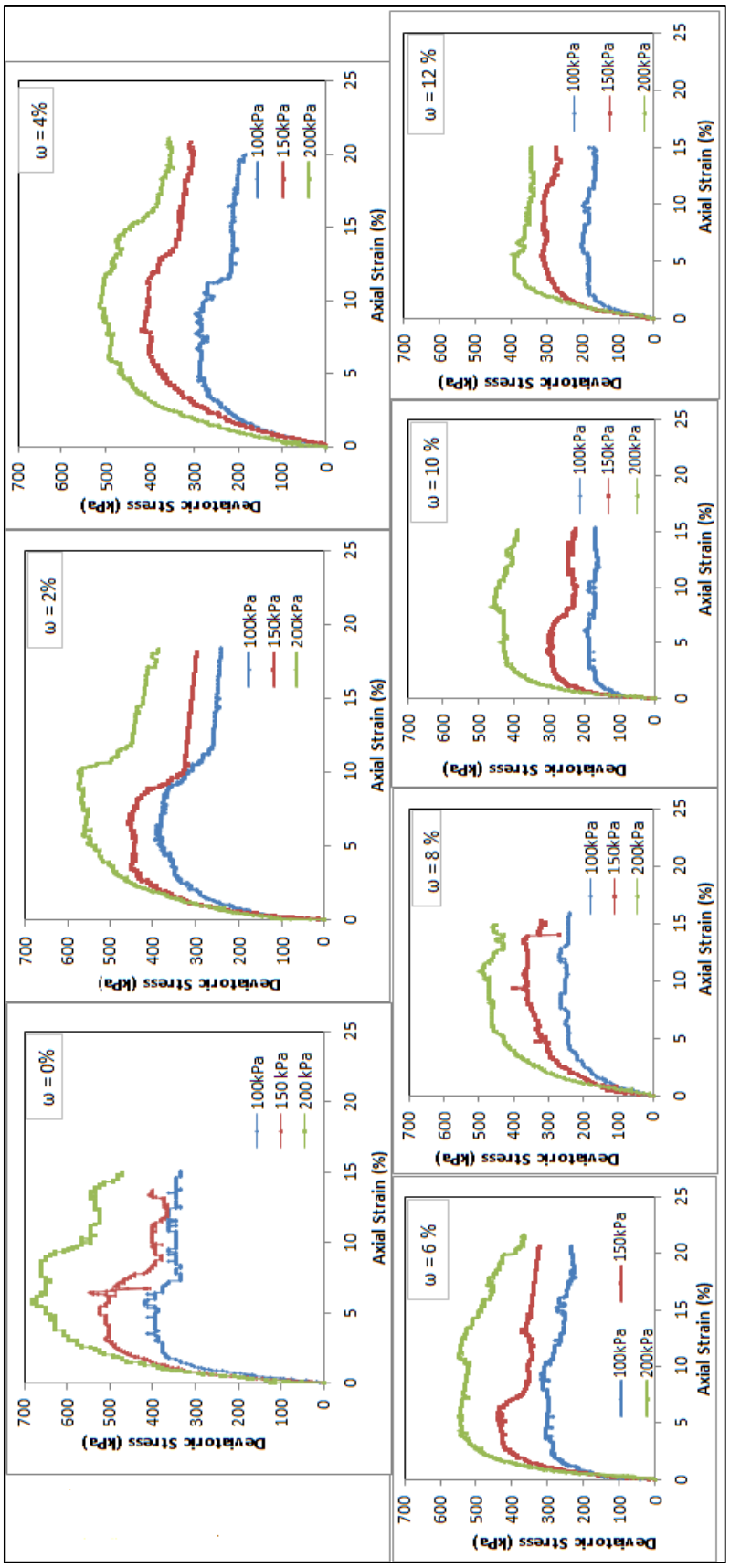

Fig. 3.10 Stress-strain curves of clean and contaminated Guwahati sands obtained under consolidated drained triaxial tests

3.6 Mineralogical studies

3.6.1 X-Ray Diffraction Studies

X-ray diffraction studies were conducted to help in determining whether interaction of sand with crude oil at different dosages leads to any mineralogical changes. The samples were scanned from $5^{o}2\theta$ to $80^{o}2\theta$. The mineral compositions were determined using XRD peak positions and intensities. Fig. 3.11 shows the X-ray diffraction patterns for uncontaminated and contaminated sand. It was evident from the figures that there was no significant change in the mineral compositions due to oil interaction. The position of the corresponding peaks of the minerals remained unchanged.

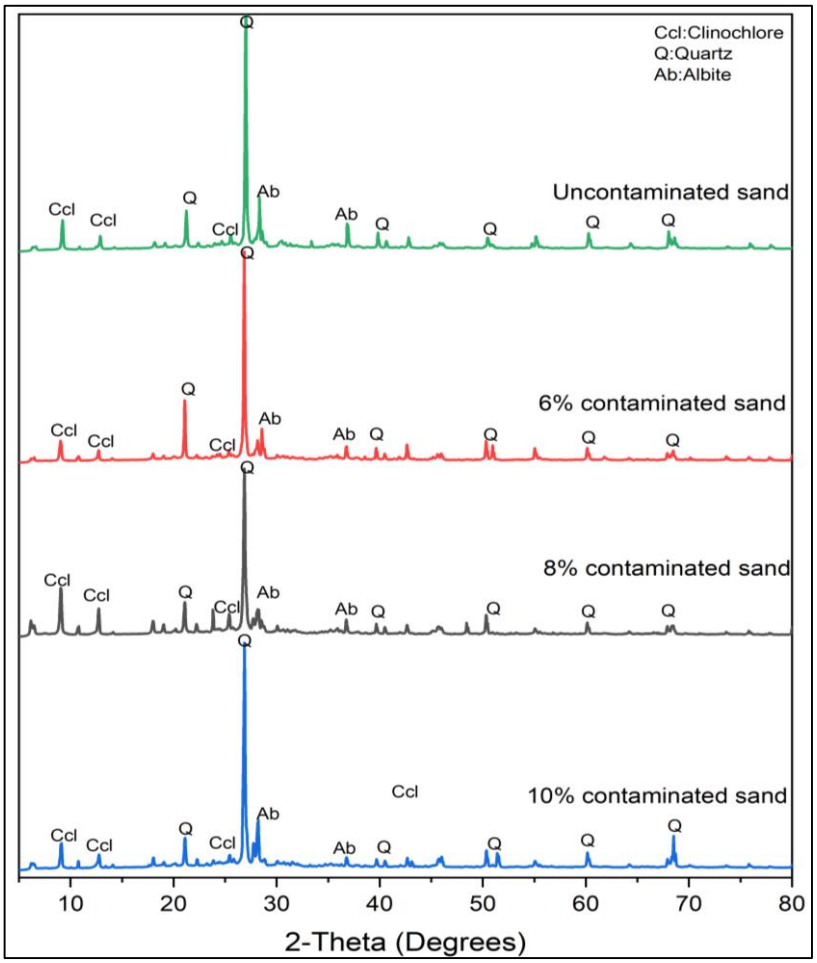

Fig. 3.11 X-ray diffraction patterns of uncontaminated sand and crude oil contaminated sand

3.6.2 Fourier Transform Infrared Spectroscopy (FTIR)

FTIR spectra of uncontaminated and crude oil contaminated sand have been shown in Fig. 3.12. The results have been plotted in terms of percentage transmittance. The characteristic peaks of hydrocarbons (crude oil) have been identified in the range of 2900–3000 cm^{-1} (Okparanma et al. 2011) where a significant dip in the peaks of the derived transmittance due to oil contamination was observed. This peak was directly related to the concentration of the petroleum hydrocarbons present in the sand. For higher concentration of hydrocarbon contamination, lower transmittance peaks were observed.

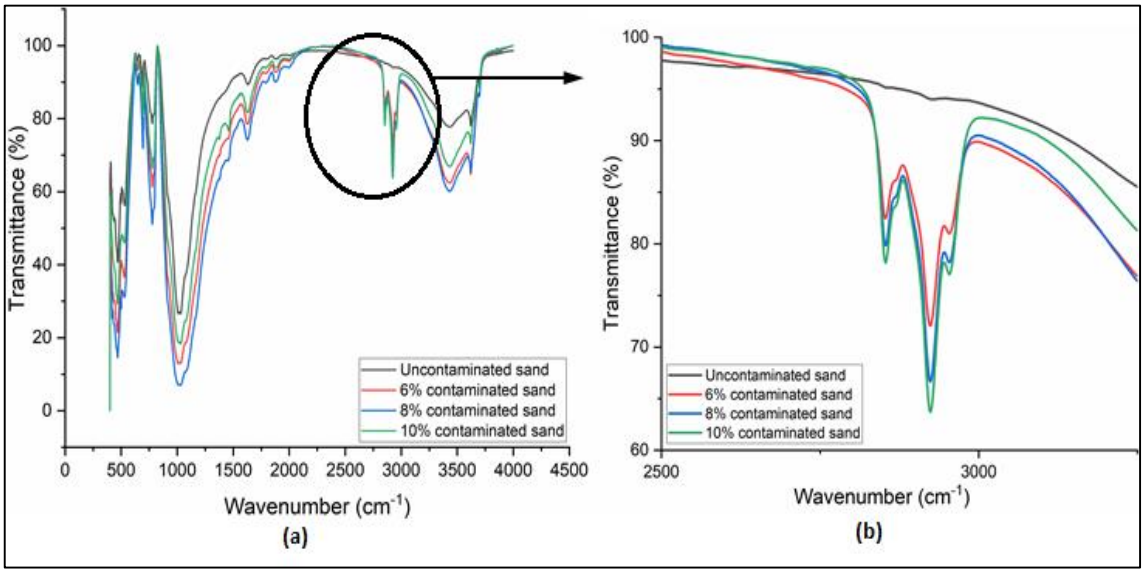

Fig. 3.12 FTIR analysis results of hydrocarbon contaminated Guwahati sand

3.7 Morphological Studies

3.7.1 Scanning Electron Microscopy

In Fig. 3.13, an attempt was made to precisely consider the effects of crude oil contamination on the microstructural characteristics of sand by comparing the SEM images of both clean and contaminated sand. It was evident from the figures that at lower degree of contamination (≤ 6%), oil droplets occupied the inter-granular spaces but does not completely coats the sand grains. On the other hand, at higher contamination (>8%), a layer of crude oil was observed

over the sand grains which may completely cut-off the grain to grain contact in the sand matrix.

3.7.2 Volumetric Oil Content

To cater further justification to the SEM observations, Fig. 3.14 presents the volumetric oil content, expressed as the percentage of pore volume occupied by the oil, under each percentage of contamination. The detailed procedure to determine the volumetric oil content has been incorporated in Appendix A. It is apparent from the figure that at 2% oil content, 7% of the total pore volume was occupies with oil. On the other hand, at 10% oil content, this volumetric oil content was 28%. Hence, with increasing oil content the percentage pore volume occupied by the oil also increases.

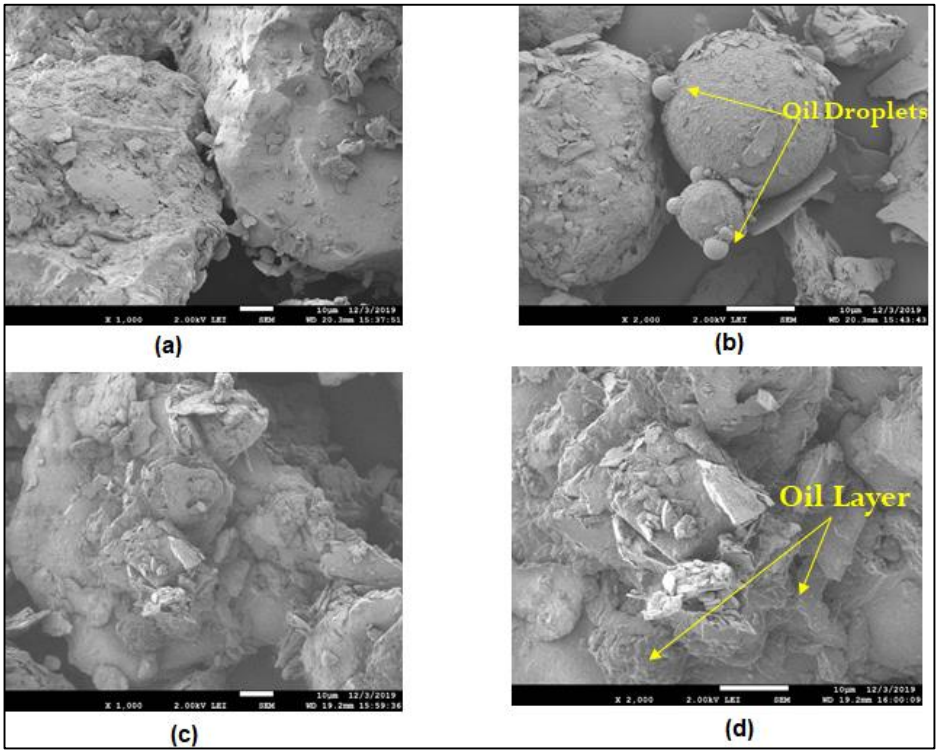

Fig. 3.13 Scanning electron microscopy images for (a) uncontaminated sand (b) 4% contaminated sand (c) 8% contaminated sand and (d) 10% contaminated sand under x1000 magnification

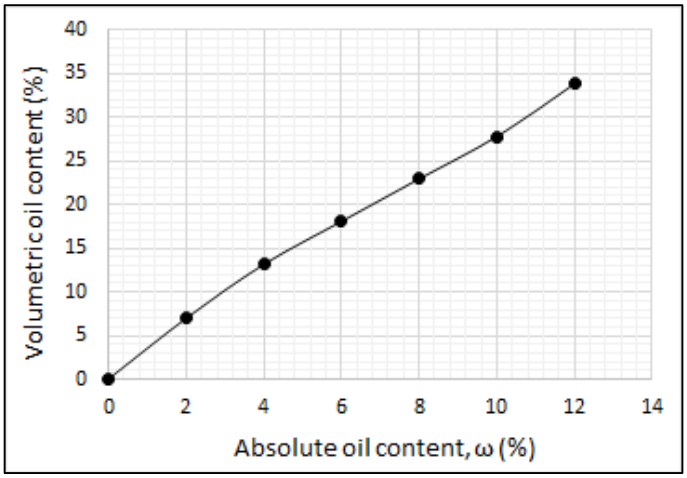

Fig. 3.14 Volumetric oil content versus absolute oil content

3.8 Methods of Liquefaction Assessment

Several methods for assessing liquefaction potential have been established among which the cyclic stress and cyclic strain approaches are widely used to evaluate the liquefaction resistance of soils in both laboratory and field tests. In cyclic stress approach, both loading and liquefaction resistance are characterized in terms of cyclic stresses. On the other hand, in cyclic strain approach, both loading and liquefaction resistance are characterized by cyclic strains.

Fig. 3.15 shows a chart categorizing various methods that can be employed to evaluate liquefaction potential of soils. In general, liquefaction evaluation methodologies can be categorized into four groups, with the laboratory-based technique, field-based approach, and shear wave velocity (V_s) based technique being the most extensively utilized. Cyclic triaxial test, cyclic simple shear and cyclic torsional test are some commonly used laboratory techniques. 1-g shaking table and centrifuge testing are used for laboratory testing on a larger scale and in a more realistic manner. Further, Standard Penetration Test (SPT), Cone Penetration Test (CPT), Dilatometer Test, etc. are some of the in-situ techniques used to

evaluate liquefaction resistance. Although, penetration based methods are well developed, it is sometimes impractical to conduct such tests. In such cases, shear wave velocity offers a great alternative to evaluate liquefaction resistance of soils. Bender element test and Resonant column test are widely used laboratory based method to calculate shear wave velocity. In-situ measurement methods of shear wave velocity include multichannel analysis of surface waves, micrometer analysis etc. These measured shear wave velocities are the related to the liquefaction potential as per established and validated correlations. Besides the above mentioned approaches, there are certain approaches such as energy dissipation method and response analysis which are also being used in the evaluation of liquefaction potential.

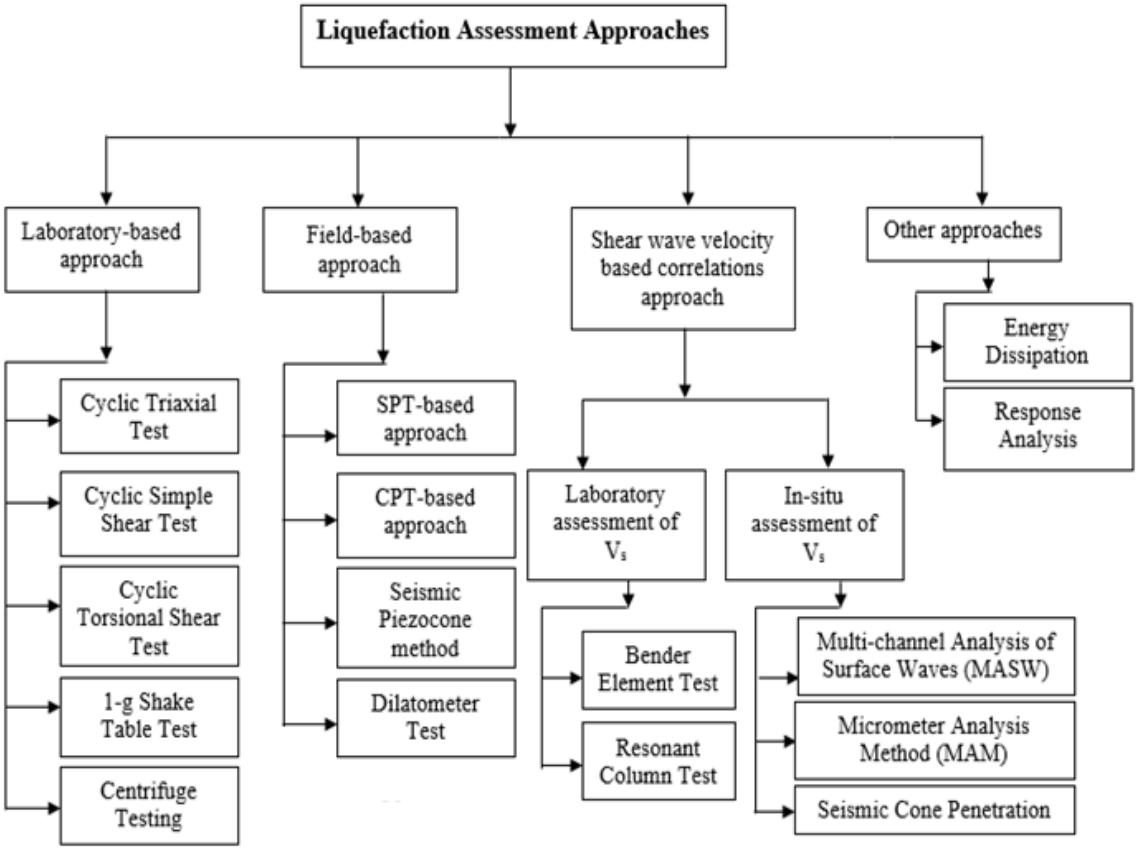

Fig. 3.15 Liquefaction analysis approaches

3.8.1 Cyclic Triaxial Test

Cyclic triaxial test is a widely recommended test for the study of soil liquefaction. This test can reveal the manner in which excess pore pressure is generated. On the basis of the results from undrained cyclic triaxial test data, the pore water pressure buildup can be evaluated. Failure initiation in a sample has been subjectively defined. Several failure criteria for cyclically loaded specimens have been proposed by many studies.

3.8.1.1 Pore Water Pressure based criterion

Pore Pressure based criterion defines the complete liquefaction state when the pore pressure ratio reaches unity. In a triaxial compression test, this occurs when the excess pore water pressure increase (Δu) equals the initial effective minor principal stress. Pore water pressure criteria capture several important aspects of the liquefaction mechanism, and as a result, it appeals to the researchers.

3.8.1.2 Strain/Deformation Based Criterion

This criterion suggested that the attainment of threshold strain can be used to assess the potential for manifesting liquefaction. According to the National Research Council (1985), all the events involving excessive deformation of saturated cohesionless soils be referred to as "liquefaction," although Seed and Lee (1966) distinguished between "liquefaction" and "failure". They proposed that a soil is assumed to have liquefied when its resistance to deformation is zero throughout a wide range of strain amplitude, and a soil is regarded to have failed when applied stresses cause excessive deformations. Ishihara recommended 5% double amplitude strain as the threshold strain for soil failure.

3.8.2 Liquefaction Assessment using Bender Element Test

Field evaluation of liquefaction resistance can be done through the empirical charts which have been established relating liquefaction resistance with the in-situ shear wave velocity. Several empirical charts correlating the liquefaction resistance and shear-wave velocity have been developed and used in practice for evaluating the liquefaction potential of soils in the field. Simatupang et al. (2018) described the procedure for assessing the liquefaction potential from laboratory measured shear wave velocity. The laboratory measured shear wave velocity V_{s_iso} in the isotopically confined soil should be adjusted to the field condition (V_s) as per eq. (3.2)

$$V_s = V_{s\_iso} \left(\frac{1+2K_0}{3}\right)^{0.25} \tag{3.2}$$

where K_0 is the coefficient of the horizontal earth pressure at rest. Similarly, liquefaction resistance obtained from the laboratory cyclic test at isotropic condition R_L should also be transformed to the cyclic-resistance ratio (CRR) for the field conditions as per eq. (3.3)

$$CRR = R_L \left(\frac{1+2K_0}{3}\right) \tag{3.3}$$

These combinations of V_{s1}-CRR can then be plotted on the chart proposed by Andrus and Stokoe (2000) and has been shown in Fig 2.13. From the chart, it can be easily identified whether the soil is prone to liquefaction or not. In general, it can be inferred from the chart that increase in shear wave velocity increases the liquefaction resistance. Therefore, in reference to the present study, laboratory measurement of shear wave velocities using bender element test will provide an indicative assessment of the liquefaction resistance of the Guwahati sand.

3.8.3 Liquefaction Assessment through 1g-shake table testing

Shake table test is yet another laboratory approach for determining liquefaction potential that, when compared to other small scale studies, more nearly resembles field conditions. It involves model testing with close monitoring of pore water pressure, acceleration and displacements caused by specified input motion. Liquefaction assessment in shake table test is also based on the pore pressure ratio (r_u) criterion where $r_u \geq 1$ indicates complete liquefaction. At this stage, dynamically induced pore water pressure exceeds the effective overburden pressure.

3.9 Methodology Adopted

This section succinctly explains the methodology that has been adopted to meet the primary objectives of this study. Fig. 3.16 shows a line chart sequentially depicting the steps employed in the study. Broadly, the methodology comprises of soil sampling from the concerned sites followed by assessment of their relative liquefaction susceptibility based on the widely used Chinese criterion and selection of the most liquefiable soil. Then an extensive series of experiments were conducted and the recorded data were analyzed.

The whole experimental program was conducted in three phases. In the first phase, Bender element test was conducted to determine the effect of degree as well as depth of crude oil contamination on the shear wave velocity of Guwahati sand. It will provide an indicative assessment of crude oil content on the liquefaction potential of the sand. In the second phase, a series of shake table tests were executed to simulate the field liquefaction phenomenon at laboratory scale. Again, the effect of degree and depth of contamination on the pore pressure-time histories were determined under sinusoidal base shaking. In addition, the effect of shaking histories on the pore pressure response were also studied. In the third phase, cyclic

triaxial tests were conducted on clean and contaminated Guwahati sand to evaluate the effect of hydrocarbon on the liquefaction behavior of Guwahati sand. Further, an EICP stabilization technique was designed to improve the dynamic behavior of contaminated sand. The efficiency of this EICP technique was investigated cyclic loading. Coupled effect of hydrocarbon content and curing period on the degradation index and cyclic pore pressure response was analyzed.

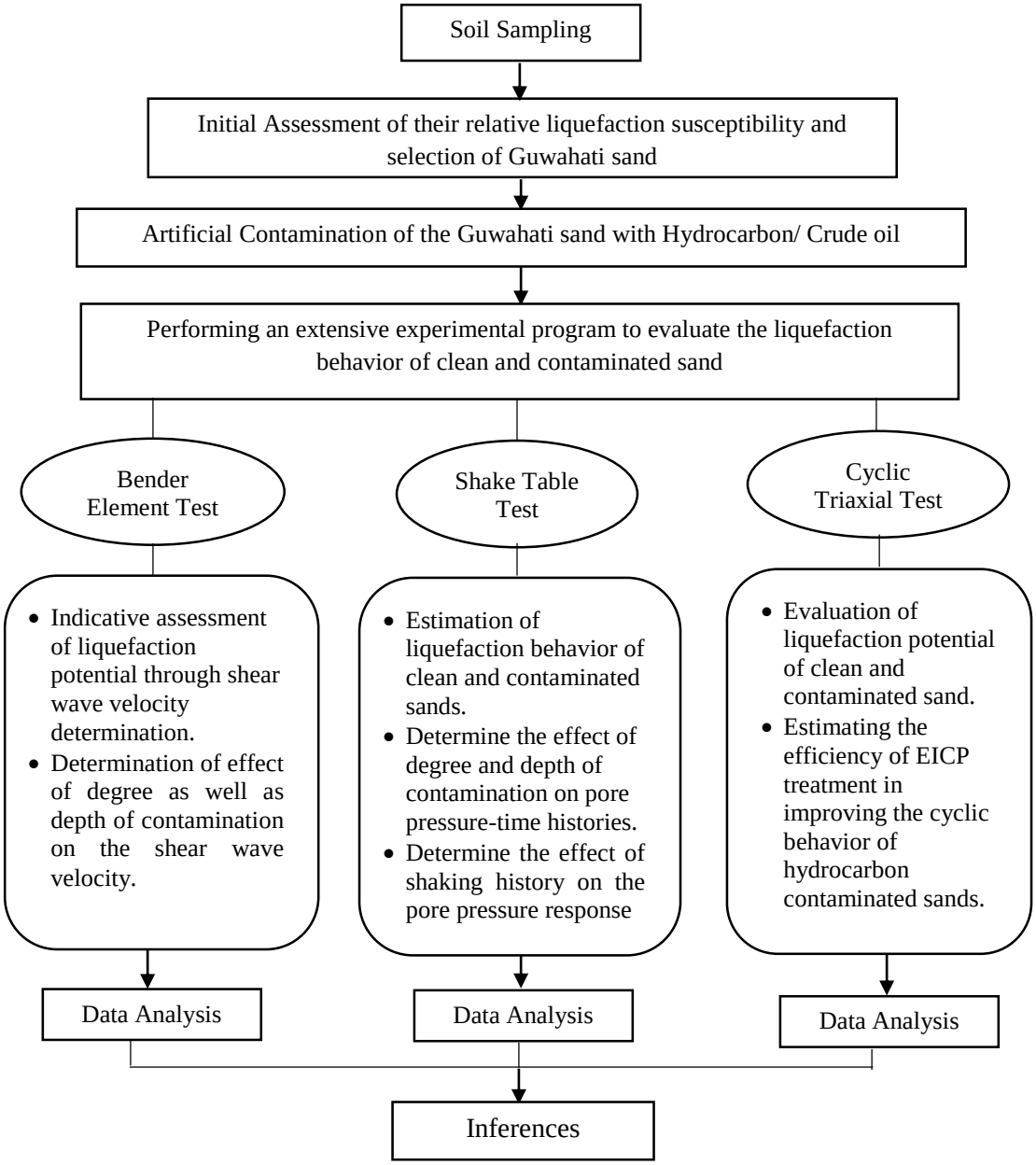

Fig. 3.16 Workflow chart for research methodology

3.10 Summary

The chapter has described the details of materials along with their relevant properties in detail. Various approaches for evaluating liquefaction potential were discussed specifically highlighting the methodologies adopted. Their experimental setup, procedures and results have been discussed in detail in the subsequent chapters.